

New coloured coatings to enhance silica sand absorbance for direct particle solar receiver applications

Gimeno-furio, A.; Hernandez, L.; Martinez-cuenca, R.; Mondragón, R.; Vela, A.; Cabedo, L.; Barreneche, C.; Lacob, M.

DOI:

[10.1016/j.renene.2020.01.053](https://doi.org/10.1016/j.renene.2020.01.053)

License:

Creative Commons: Attribution-NonCommercial-NoDerivs (CC BY-NC-ND)

Document Version

Peer reviewed version

Citation for published version (Harvard):

Gimeno-furio, A, Hernandez, L, Martinez-cuenca, R, Mondragón, R, Vela, A, Cabedo, L, Barreneche, C & Lacob, M 2020, 'New coloured coatings to enhance silica sand absorbance for direct particle solar receiver applications', *Renewable Energy*, vol. 152, pp. 1-8. <https://doi.org/10.1016/j.renene.2020.01.053>

[Link to publication on Research at Birmingham portal](#)

General rights

Unless a licence is specified above, all rights (including copyright and moral rights) in this document are retained by the authors and/or the copyright holders. The express permission of the copyright holder must be obtained for any use of this material other than for purposes permitted by law.

- Users may freely distribute the URL that is used to identify this publication.
- Users may download and/or print one copy of the publication from the University of Birmingham research portal for the purpose of private study or non-commercial research.
- User may use extracts from the document in line with the concept of 'fair dealing' under the Copyright, Designs and Patents Act 1988 (?)
- Users may not further distribute the material nor use it for the purposes of commercial gain.

Where a licence is displayed above, please note the terms and conditions of the licence govern your use of this document.

When citing, please reference the published version.

Take down policy

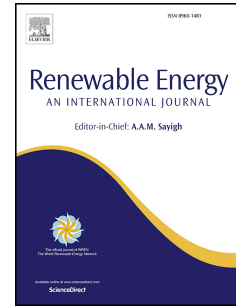
While the University of Birmingham exercises care and attention in making items available there are rare occasions when an item has been uploaded in error or has been deemed to be commercially or otherwise sensitive.

If you believe that this is the case for this document, please contact UBIRA@lists.bham.ac.uk providing details and we will remove access to the work immediately and investigate.

Journal Pre-proof

New coloured coatings to enhance silica sand absorbance for direct particle solar receiver applications

A. Gimeno-Furio, L. Hernandez, R. Martinez-Cuenca, R. Mondragón, A. Vela, L. Cabedo, C. Barreneche, M. Iacob



PII: S0960-1481(20)30058-6

DOI: <https://doi.org/10.1016/j.renene.2020.01.053>

Reference: RENE 12915

To appear in: *Renewable Energy*

Received Date: 21 June 2019

Revised Date: 24 December 2019

Accepted Date: 11 January 2020

Please cite this article as: Gimeno-Furio A, Hernandez L, Martinez-Cuenca R, Mondragón R, Vela A, Cabedo L, Barreneche C, Iacob M, New coloured coatings to enhance silica sand absorbance for direct particle solar receiver applications, *Renewable Energy* (2020), doi: <https://doi.org/10.1016/j.renene.2020.01.053>.

This is a PDF file of an article that has undergone enhancements after acceptance, such as the addition of a cover page and metadata, and formatting for readability, but it is not yet the definitive version of record. This version will undergo additional copyediting, typesetting and review before it is published in its final form, but we are providing this version to give early visibility of the article. Please note that, during the production process, errors may be discovered which could affect the content, and all legal disclaimers that apply to the journal pertain.

© 2020 Published by Elsevier Ltd.

Credit Author Statement

A. Gimeno-Furio: Formal analysis, Resources , Writing, L. Hernandez: Methodology, Formal analysis, Writing, R. Martinez-Cuenca: Visualization, R. Mondragón: Validation, A. Vela: Validation, L. Cabedo: Writing, Validation, C. Barreneche: Conceptualization, Writing , M. Iacob: Validation

Journal Pre-proof

New coloured coatings to enhance silica sand absorbance for direct particle solar receiver applications

A. Gimeno-Furio¹, L. Hernandez^{1*}, R. Martinez-Cuenca¹, R. Mondragón¹, A. Vela¹, L. Cabedo², C. Barreneche^{3,4}, M. Iacob⁵

¹ Department of Mechanical Engineering and Construction, Universitat Jaume I, Castelló de la Plana, Spain

² Polymers and Advanced Materials Group (PIMA), Universitat Jaume I, Castelló de la Plana, Spain

³ Department of Materials Science and Physical Chemistry, Universitat de Barcelona, Barcelona, Spain

⁴ Birmingham Centre for Energy Storage & School of Chemical Engineering, University of Birmingham, United Kingdom

⁵ Petru Poni Institute of Macromolecular Chemistry Iasi, Romania

*Corresponding author: lhernand@emc.uji.es

Abstract

New systems using solid particles for solar energy capturing, heat transfer and thermal energy storage have been proposed and analysed in direct particle solar receivers. In this work, black coloured silica sand was investigated as a possible solid particle for such combined systems. Two different methods based on a carbon coating approach were implemented to black colour the initial material to improve their solar absorption characteristics. The morphology of the raw and coloured sands was analysed by scanning electron microscopy (SEM), particle size characterisation and porosity measurements. The coating of the black-coloured silica sands was evaluated by thermogravimetry. Solar absorption was characterised in a double-beam UV-VIS spectrophotometer combined with an integrating sphere, and with enhancements of approximately 100%, found for both coloured sands. The thermal storage and heat transfer capabilities of the initial and coated sands were measured at different temperatures. Some improvements in the specific heat capacity and reductions in thermal conductivity due to porosity changes were observed.

Key words: Solar energy, particle solar receivers, nanoparticles, silica sand, absorption, thermal conductivity

41 1. INTRODUCTION

42 The increasing demand of energy together with the present scenario of climate change
43 concerns and decreasing available fossil fuel resources have motivated a rapid
44 deployment, development and implementation and improvements of solar thermal
45 receiver technologies. However, additional increases of the efficiency power cycles and
46 reduction of the levelized cost of energy of these systems are being investigated, and
47 Particle Solar Receivers (PSR) have been identified as an interesting option [1].

48
49 PSR use solid particles that are heated by concentrated solar radiation and, apart to be
50 used as heat transfer media, may be used to store energy. In contrast with
51 conventional solar receivers, PSR present some advantages as [2]: wide range of
52 operating temperatures (beyond 600 °C without corrosion and below 200 °C without
53 freezing risks as in molten salts), higher power efficiencies due to higher operating
54 temperatures, direct storage of heat transfer media for energy production beyond solar
55 hours, and use of relatively inexpensive and inert working media.

56
57 Two main PSD have been developed: direct and indirect. Direct PSD where the
58 radiation is directly absorbed by the material and indirect PSR, in which certain
59 surfaces are used to confine and also heat the particles. Comparative analysis of
60 different configurations of direct PSR (free falling, obstructed, centrifugal, fluidized
61 configurations) and indirect PSR (gravity driven flow through enclosures, fluidized flow
62 through tubes, etc) have been recently published [3,4].

63
64 Directly heated particle receivers present the advantage that the media is directly
65 irradiated, eliminating the heat transfer resistance between heated surfaces and
66 particles and therefore reducing exergy losses [5-10]. Several direct PSR projects have
67 been developed at lab or pilot scales since early 1980s [10-15]. Desirable properties of
68 the particles used for direct PSD include high solar absorptance, low cost, wide
69 availability, high heat capacity and durability among others [16]. A variety of particles
70 have been analysed and tested for direct PSD [4], including ceramic particles [17],
71 silicon carbide [18], bauxite [8], alumina [14] and sand [10, 19, 20]. Sand is an
72 inexpensive and abundant media in attractive locations for solar projects; however its
73 solar absorptance is low.

74
75 In this work, sand has been black coloured via two different methods in order to
76 improve the absorption capability of the natural sand, one using carbon black (CB)
77 nanoparticles and the other through glucose degradation. The black coating was
78 characterized, including thermal stability at high temperatures. In order to assess the
79 potential of these materials as candidates for direct PSR, different relevant properties
80 of the coloured sand, as solar absorption, thermal conductivity and specific heat
81 capacity were measured and compared to the raw particles.

83 2. Materials and methods

84 2.1. Materials

85 The base material herein studied is silica sand from open-cast mining in Spain.
86 According to the supplier (Silice Gllaranz), sand contains more than 99% SiO₂.

87 The materials used to produce the coating are carbon black (CB) nanoparticles
88 (ELFTEX 570 from Cabot Corporation), anhydrous glucose (Scharlau) and acetone
89 (Guinama). They were all used as received.

90

91 **2.2. Coloured sand preparation**

92 Raw sand was black-coloured by two different methods based on a carbon coating
93 approach. Both methods are described and experimentally compared below. All the
94 mass measurements were taken on an analytical balance during sample synthesis
95 (Kern ABS, ± 0.001 mg).

96 **2.2.1. Carbon black coating**

97 The first synthesis method to colour sand was based on a carbon black coating. These
98 coloured samples were obtained by suspending 3 grams of carbon black nanoparticles
99 in 240 ml of acetone. The CB nanoparticles were selected by their colour, thermal and
100 chemical stability, and low price. According to the manufacturer, CB nanoparticles are
101 spherical and have an average primary diameter of 10 nm. In order to achieve a good
102 suspension, the mixture was sonicated with an ultrasonic probe (Sonoplus HD2200,
103 Bandelin) for 40 seconds at medium-high power. Then 60 grams of silica sand were
104 added and dispersed in the CB suspension using an ultrasonic probe for 30 seconds at
105 high power. The resulting suspension was poured into a Petri dish and allowed to dry in
106 an oven (Digitronic 2005141, J.P. Selecta, SA) at 100°C for 15 minutes. In this paper,
107 the coloured samples using this method are denoted as CB sand.

108

109 **2.2.1. Glucose degradation coating**

110 The second synthesis method to colour sand was based on the generation of a char
111 coating over sand by anaerobic thermal degradation of glucose, where a mixture of
112 70% sand and 30% glucose in weight was prepared. Distilled water was poured on the
113 vessel to cover the sample and the mixture was stirred for 35 minutes at 55°C to
114 ensure that glucose was fully dissolved. Water was evaporated by drying thin layers of
115 suspension in an oven at 100°C. Finally, the dried mixture was placed inside a muffle
116 furnace at 400°C for 10 minutes at a constant N₂ flow rate to ensure anaerobic
117 atmosphere conditions. This thermal treatment causes glucose graphitisation and
118 results in a black char coating on sand particles. In this paper, the coloured samples
119 using this method are denoted as Glucose sand.

120

121 **2.3. Experimental characterisation**

122 **Scanning electron microscopy**

123 Scanning electron microscopy (SEM) was performed by JEOL 7001F and JEOL JSM-
124 6510 microscopes equipped with digital image acquisition. Powder samples were
125 observed and the materials' morphology and size were determined. In order to
126 characterise the coatings formed on sand grains, secondary electro images and digital
127 image processing were used.

128 **Particle size**

129 Volume particle size distribution was measured using a laser diffraction analyser
130 (Mastersizer 2000, Malvern). Efficient sample dispersion helps to ensure that the
131 particle size data measured by a laser diffraction analyser are both representative and
132 relevant [21]. Particle size distribution was characterised by volume fraction diameter
133 d_{50} , which is the value of the particle diameter at 50% in cumulative distribution.

134 According to the manufacturer, the error for the equipment of d_{50} is 3%. Measurements
135 were taken of raw sand and two black-coloured sand samples.

136 Porosity

137 Porosity (ε) was calculated with Equation 1:

$$138 \quad \varepsilon = \frac{\rho_r - \rho_b}{\rho_r} \quad \text{Eq. 1}$$

139 where ρ_r is the real density of the sample under study (kg/m^3) measured with a Helium
140 Pycnometer from Micrometrics, and ρ_b is the bulk density of the same sample (kg/m^3)
141 measured by the volume and mass of samples.

142 Thermogravimetric analysis

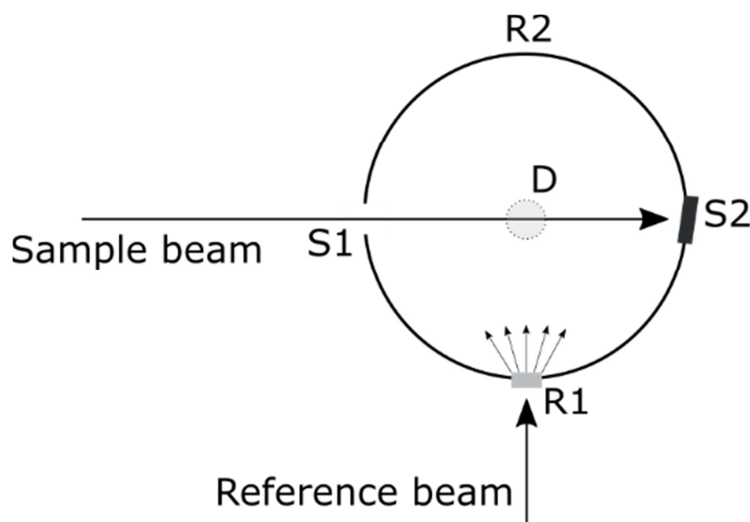
143 A thermogravimetric analysis (TGA) was performed to evaluate the stability of raw sand
144 and also the sand coating in both colouring methods. Tests were run in a
145 thermogravimetric device (Model Simultaneous SDTQ600, TA Instruments) at a
146 synthetic air flow of 50 ml/min. For each sample, around 40 mg were analysed in 100
147 μL alumina crucibles at a constant heating rate of 10 C/min between 100°C and
148 1,000°C.

149 Spectrophotometer

150 The absorption spectrum is one of the most important properties studied herein as it
151 determines the amount of energy absorbed by the pure, CB and glucose sand
152 samples. A UV-Vis-NIR spectrophotometer (CARY 500, Varian Dev) with an integrating
153 sphere was used to measure the absorption spectrum of each sample. This equipment
154 allows spectral measurements to be taken between 250 nm and 2500 nm thanks to two
155 interchangeable lamps [22]. To minimise any effects of undesired reflections and
156 absorptions, the sand samples were placed inside a quartz cuvette with a planar
157 interface (75x25x5 mm).

158 Figure 1 illustrates the detection geometry of the integrating sphere. Two laser beams
159 are directed to the sphere, one directed to the sample itself and a second acts as a
160 reference. Once the beams enter the sphere, they impact its inner Teflon surface and
161 undergo many internal reflections before being captured by the photodetector (D) at the
162 top of the integrating sphere. Note that the reference beam enters the sphere through a
163 diffusing window (R1) to reduce any losses that might arise from a direct reflection at
164 R2. This beam monitors the laser power changes that occur during the measurement
165 time required for a full wavelength scan. The sample beam enters the integrating
166 sphere through a hole in port S1 and impinges directly onto port S2. In practice, the
167 sample can be placed in either of the two ports, depending on the desired property to
168 be measured. In order to obtain the absorption spectrum, three measurements are
169 needed.

170



171

172 **Figure 1. A scheme of the integrating sphere, including the reference and sample**
 173 **beam paths and the measuring port locations (S1 and S2)**

174 The first measurement, named the baseline, is performed by leaving port S1 open and
 175 closing port S2 with a Teflon cap. Note that port S2 is tilted about 3° in relation to the
 176 normal direction to prevent the direct loss of its specular reflection through port S1. In
 177 this configuration, the sample beam enters the integrating sphere, hits the wall and
 178 undergoes many reflections before being detected. The intensity at measured the
 179 photodetector, I_0 , is proportional to the total light power of the sample beam.

180 For the second measurement, the cuvette with the sample is placed at port S1 and the
 181 tilted Teflon cap at port S2. In this configuration, the sample beam first passes through
 182 the cuvette with the sample, and the light that emerges on the other side enters the
 183 integrating sphere through S1, hits S2 and undergoes many reflections before being
 184 detected. The resulting signal intensity, I_{T+FS} , is proportional to the light power that is
 185 either directly transmitted through the sample or suffers forward scattering.

186 In the last measurement, port S1 is left open and the Teflon cap is replaced with the
 187 cuvette with the sample at port S2 (the cuvette is also tilted 3° in relation to the
 188 normal direction). The resulting signal, I_{R+BS} , is proportional to the sum of the reflected and
 189 backward scattered light powers.

190 Once the three above-mentioned spectrums are measured, absorption spectrum (A) of
 191 the sample is obtained through Equation 2:

$$192 \quad A (\%) = \frac{I_0 - I_{T+FS} - I_{R+BS}}{I_0} \cdot 100 \quad \text{Eq. 2}$$

193 The measured spectrum range was selected to lie between 400 nm and 1,500 nm with
 194 a spectral resolution of 0.5 nm, the 800 to 1,100 nm range was excluded due to the
 195 limitations in the experimental set-up caused by the lamps switch and the coupling of
 196 both equipments. This range includes visible and part of the near infrared to avoid
 197 unreliable spectral ranges of the equipment and comprises 53% of the total solar
 198 radiation energy reaching the Earth, including the highest solar radiation level.

199 **Differential scanning calorimetry**

200 Specific heat capacity (C_p) was performed to know the validity of the sample as a
 201 thermal energy storage material. C_p was measured using a Differential Scanning
 202 Calorimeter (DSC; Model DSC882e Mettler Toledo). Around 15 mg of each sample

203 were used to run the analyses in 40- μ L aluminium crucibles. As the material can
204 undergo oxidation by air, the test was done at a 50 ml/min constant N₂ flow rate
205 between 300°C and 500°C with consecutive isothermal segments and the temperature
206 difference between isotherms of 1°C. Therefore, Cp was measured at 300, 400, and
207 500°C. After completing measures, the specific heat capacity was calculated by
208 applying the Areas Methods described by Ferrer et al. [23], which presents relative
209 errors under 4%. The measure was repeated 3 times and the differences found in
210 these three cycles were always less than a 5% relative error. These findings show the
211 reliability of the experimental data.

212 **Conductimeter**

213 The thermal conductivity (k) of all the samples was measured in a KD2 Pro
214 conductimeter (Decagon Devices Inc.). KD2 Pro is a commercial device that measures
215 thermal conductivity by the transient hot wire technique. This technique is based on
216 measuring the temperature/time response of the wire to an electrical pulse. The wire is
217 inserted vertically into the solid sample, which was placed inside a metal tube (70 g).
218 To run the test under high-temperature conditions, the tube was placed in an oven,
219 where temperature was controlled. The test was done at room temperature, 40°C, 80°C
220 and 120°C. Before any testing started, a 1-hour period was needed for the sample to
221 reach the desired temperature. Afterwards, five measurements were taken for all the
222 samples at each temperature. The experimental error was statistically obtained at a
223 95% of confidence level, with an average error of 2.85%.

224

225 **3. RESULTS AND DISCUSSION**

226 **3.1. Silica sand morphology and coating**

227 All the samples under study are shown in Figure 2 to illustrate the difference in colour
228 terms. This is the first time that sand is coloured by this procedure to improve the
229 absorptivity properties and to enhance its direct use as TES materials.

230

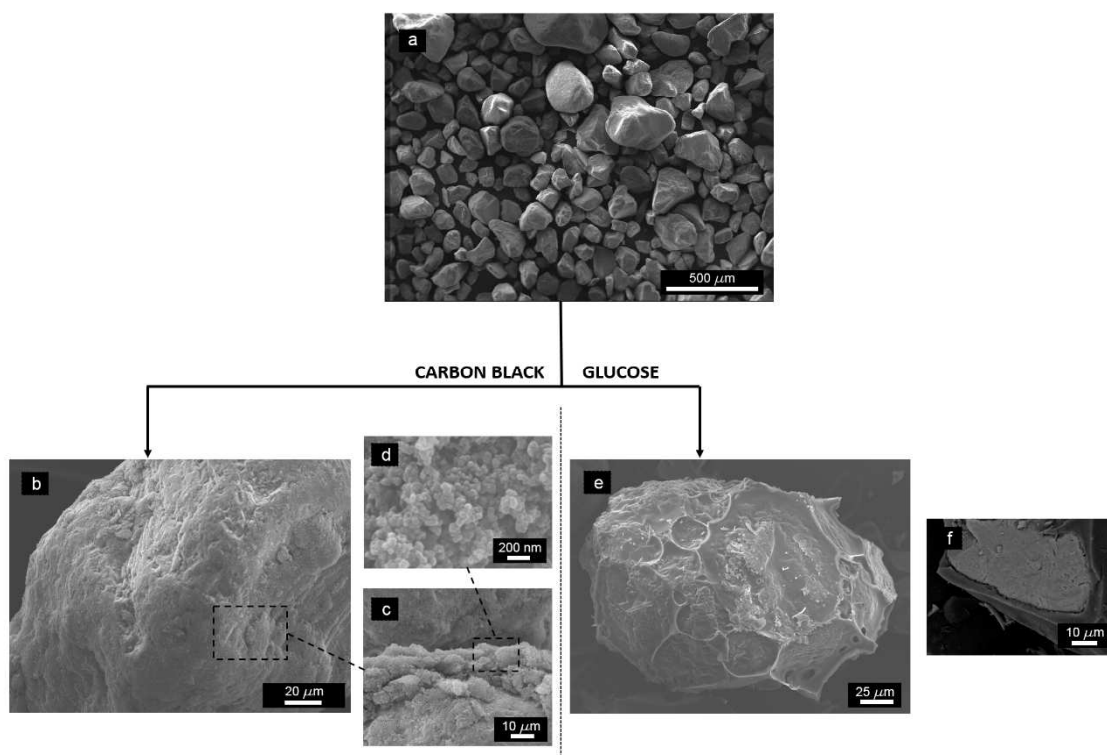


231

232 **Figure 2. Pure sand, CB sand and Glucose sand (from left to right)**

233

234 Figure 3 shows the SEM images herein obtained for raw sand and both coated sample
235 types.



236
 237 **Figure 3. Morphology of sand and carbon-coated sand. (a) SEM micrograph of pristine**
 238 **sand. (b) Carbon black-coated sand granule. (c) Detail of the CB coating. (d) High**
 239 **magnification detail of the carbon black nanoparticles. (e) Glucose-coated sand granule.**
 240 **(f) Detail of the glucose coating.**

241

242 Figure 3a shows an SEM micrograph of the sand particles as delivered. Sand particles
 243 present a spherical geometry with a smooth regular surface given its natural origin. The
 244 average d_{50} particle size is 294 μm , as determined by the Mastersizer equipment.
 245 Figure 3b presents a CB-coated sand granule, which is fully covered by a
 246 homogeneous coating to, thus, present a smooth surface with minor roughness. This
 247 uniform coating is formed by myriads of carbon black nanoparticles to form a thick
 248 layer. This layer is the result of the agglomeration of CB nanoparticles during the drying
 249 process, so that when acetone is fully removed, the carbon nanospheres tend to
 250 agglomerate and result in a well-packed layer (see Figure 3d). Nanoparticles are
 251 therefore clustered by an electrostatic interaction effect. Figure 3c shows the edge of a
 252 broken coating where the carbon black layer morphology is observed. The thickness of
 253 the layer falls within the range of tens of microns and the measured average d_{50}
 254 particle size of the CB coated particles is 343 μm .

255 A single representative sand granule coated by glucose graphitisation is presented in
 256 Figure 3e. The granule surface, unlike the CB-coated one, is very irregular, as derived
 257 from a heterogeneous char coating. A remarkable increase in surface roughness was
 258 observed due to the presence of this particular structure of ridges and valleys that
 259 derives from boiling glucose in the graphitisation step. The thickness of the coating can
 260 vary considerably from the ridges (up to several tenths of microns), while it can be less
 261 than 5 microns in the valley (see Figure 3f). The average d_{50} particle size for this
 262 coating approach is 405 μm .

263 To analyse the possible impacts of the carbon coating on sand morphology, the
 264 porosity of the different samples was evaluated. The porosity of the three sand
 265 samples was calculated by real density (ρ_r) and bulk density (ρ_b) using Eq.1. The
 266 results are shown in Table 1.

267

268 Table 1. Real and bulk densities and porosity values of the three sand samples

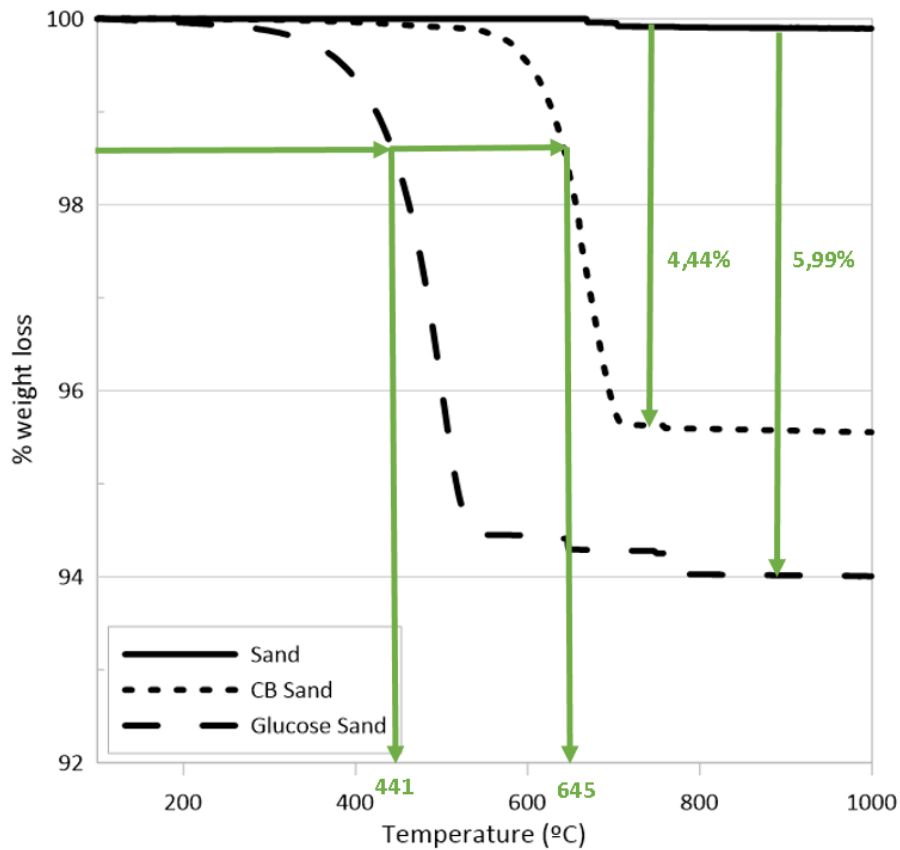
	Real density (kg/m ³)	Bulk density (kg/m ³)	Porosity (-)
Sand	2634.9	1615.5	0.387
CB Sand	2581.2	1048.9	0.594
Glucose sand	2595.5	733.3	0.717

269

270 The porosity values for the pure sand agree with those found in the bibliography [10,
 271 24], which ranged from 0.312 to 0.417. The results showed that the porosity values
 272 increased when sand was coloured. The porosity differences between both coloured
 273 sands could be due to the chemistry involved in the way the black coating was linked to
 274 sand. Therefore, the CB coating would be bonded more effectively with a smoother
 275 surface coating and fewer air cavities inside molecules because porosity was lower
 276 than in the glucose sand, where the coating surface presented more roughness.

277 The amount of carbon present in both the CB-coated and glucose-coated sands was
 278 determined by thermogravimetry at an air flow up to 1,000°C to ensure full carbon
 279 oxidation. The so-obtained mass retention vs. temperature plots are presented in
 280 Figure 4.

281 For pure sand, the small percentage of weight loss (0.1%) was associated with the
 282 impurities contained in the sample as the pure silica melting point was 1,610°C [25]. No
 283 thermal degradation was, therefore, obtained for the pure sand sample within the
 284 selected operational temperature range (100°C to 1,000°C, 10 °C/min). For both
 285 coloured sands, weight loss was associated with the degradation of the coating in the
 286 samples. As observed in Figure 4 and in both cases, carbon coating oxidation took
 287 place in a single step, although a difference in temperature appeared during this
 288 process occurs depending on the origin of carbon. The initial degradation temperature
 289 of both coloured samples is shown in the figure and was calculated as the temperature
 290 when 1.5% of weight was lost. This initial degradation temperature was read as the
 291 upper limit temperature that this material could work at without degradation. The CB-
 292 coated sample was stable for temperatures up to 645°C, while the glucose-coated
 293 ones underwent oxidation at temperatures below 441°C. Regarding the amount of
 294 carbon present in each coated sand, the CB presented a carbon content of 4.44%,
 295 while the carbon content for the glucose-coated sand was 5.99%.



296

297

Figure 4. Weight loss *versus* temperature of the sand and carbon-coated sands.

298

299

3.2. Optical characterisation

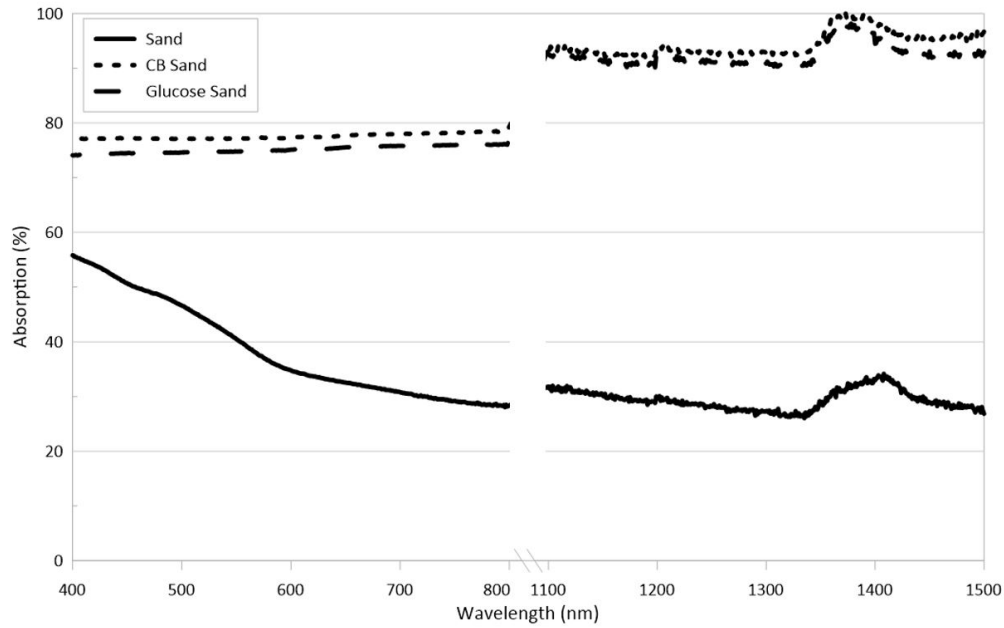
300

301

302

303

The absorption spectra of both coloured sand samples and the initial sand were evaluated to ensure that absorption improved. Figure 5 shows the absorption spectrums for the initial sand and those of the two coloured sand samples within the wavelength ranges from 400 – 800 nm and from 1,100 to 1,500 nm.



304

305

306 **Figure 5. Sand absorption spectra within the different measured wavelength ranges.**

307

308 In both the carbon-coated samples, the absorption of the coloured sand was greater
 309 than that of the pure sand over the whole spectral range. The absorption of both
 310 coloured samples was more homogeneous for different wavelengths.

311 The averaged absorption increase of the coloured sands *versus* the pure sand was
 312 more marked for the CB sand within both wavelength ranges. For the 400-800 nm
 313 wavelength range, increments of 85% and 78% were obtained for the CB and glucose
 314 sand, respectively, and these values increased to 143% and 139% for the 1,100-1,500
 315 nm range.

316 Given the possible application of sand samples in solar absorption systems, evaluating
 317 the sunlight-absorbed fraction (E) of samples was important. The sunlight absorbed
 318 fraction was considered when calculating absorption with the sand samples, following
 319 Equation 3:

$$E = \frac{\int_{\lambda_{\min}}^{\lambda_{\max}} I(\lambda) \cdot A(\lambda) d\lambda}{\int_{\lambda_{\min}}^{\lambda_{\max}} I(\lambda) d\lambda} \quad \text{Eq. 3}$$

320

321 where $I(\lambda)$ is the spectral distribution of the solar incident irradiance considered within
 322 the wavelength range (λ_{\min} , λ_{\max}) and $A(\lambda)$ is the absorption spectra. Calculations were
 323 done according to Eq. 3, by using the CIE solar spectrum with an air mass $m=1.5$ for
 324 the solar incident irradiance [26] and considering the corresponding integration bounds
 325 for each wavelength range. The results are presented in Table 2 and show the
 326 corresponding amount of solar energy that the different samples within the various
 327 wavelength ranges were able to absorb.

328

329 **Table 2. Solar energy absorbed by the three different sand samples within various**
 330 **wavelength ranges**

Sample	E (%) 400 – 800 nm	E (%) 1,100 – 1,500nm	E (%) 400 – 800 + 1,100 – 1,500 nm
Sand	43	31	40
CB Sand	79	93	82
Glucose Sand	75	92	78

331

332 The listed values agree with the absorption spectrum values as the CB sand absorbed
 333 the most, followed by glucose sand, and finally by raw sand. As a relevant result, both
 334 coloured sands approximately doubled the absorbed fraction of the solar radiation
 335 compared to the initial raw sands within the studied wavelength range.

336

337 3.3. Thermal characterisation

338 3.3.1. Specific heat capacity

339 Table 3 shows the specific heat capacity of the three different sand samples at various
 340 temperatures (300°, 400°C and 500°C).

341 As can be observed, the specific heat capacity was temperature-dependent, and the
 342 results agree with those presented by Baumann and Zunft for the raw sand values of
 343 C_p [27].

344 When sand was coated, the obtained C_p values were slightly higher. This specific heat
 345 increase with the addition of coating on sand samples can be explained by the mixture
 346 rule that applies to this property and the higher specific heat of the carbon (different
 347 allotropes present different C_p values) *versus* sand at those temperatures [28].

348 However, the C_p changes are small and close to the experimental errors, so only the
 349 global increase of specific heat with the carbon coating can be concluded.

350

351 **Table 3. Specific heat capacity of three sand samples at three temperatures**

	C_p (kJ/kg·K) at 300°C	C_p (kJ/kg·K) at 400°C	C_p (kJ/kg·K) at 500°C
Sand	1±0.02	1.07±0.03	1.14±0.02
CB Sand	1.07±0.02	1.18±0.03	1.22±0.03
Glucose Sand	1.03±0.03	1.10±0.02	1.20±0.03

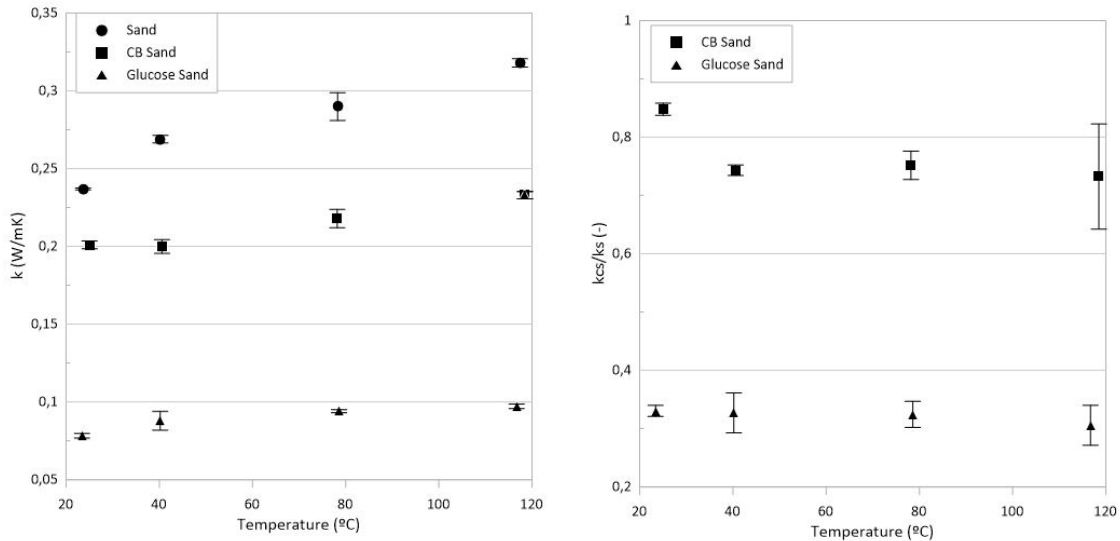
352

353

354 3.3.2. Thermal conductivity

355 The evolution of the thermal conductivity of the three samples with temperature (room
 356 temperature, 40°C, 80°C and 120°C) was measured and studied. Relative thermal
 357 conductivity was calculated by dividing coated sands and pure sand thermal
 358 conductivities (k_{CS} and k_s respectively). The evolution of thermal conductivity and its
 359 relative value for all the samples, together with the bar error corresponding to the five
 360 experimental measurements, are plotted in Figure 6.

361



362

363 **Figure 6. Evolution of thermal conductivity (left) and relative thermal conductivity with**
 364 **temperature (right)**

365 The thermal conductivity results of the raw sand presented an increasing dependence
 366 with temperature and agree with the literature [26,29]. A weaker temperature
 367 dependence was shown for the coated sand samples.

368 For both coloured sands, thermal conductivity was lower than that of the raw sand, with
 369 average decreases of 55% and 45% for the CB sand and Glucose sand, respectively.
 370 These decreases can be explained by changes in porosity.

371 When comparing the thermal conductivity values and porosity values from Table 1 and
 372 Figure 6, thermal conductivity was seen to lower and be directly related with the
 373 porosity increments. This trend was also supported by research based on studying
 374 different sand types [30]. To estimate k , a semiempirical relationship was developed by
 375 Johansen in [31]:

$$376 \quad k = \frac{0.135\rho_b + 64.7}{\rho_r - 0.947\rho_b} \quad \text{Eq. 4}$$

377 where ρ_b is the bulk density of the sand sample (kg/m^3) and ρ_r is the real density of the
 378 sample (kg/m^3). The experimental and predicted thermal conductivity values, together
 379 with the corresponding relative errors, are presented in Table 4 for the three sand
 380 samples. A good agreement is shown, which therefore confirms the relationship
 381 between thermal conductivity reduction and porosity increments.

382 **Table 4. Measured and predicted thermal conductivity values**

	Measured Thermal conductivity (W/mK)	Predicted Thermal conductivity (W/mK)	Error (%)
Sand	0.213	0.256	18.3%
CB Sand	0.113	0.130	13.9%
Glucose Sand	0.082	0.086	4.9%

383

384

385 4. CONCLUSIONS

386 This work presents two methods to colour common silica sand from Silice Gllaranz
387 (Spain) to be useful for direct absorption and TES materials in direct PSR.

388 The first was coloured by adding carbon black nanoparticles. The produced amount of
389 coating was quantified as 4.44% wt. This sample presented lower density and higher
390 porosity than the raw silica sand. The maximum working temperature for these
391 samples was 645 °C. Optical properties increased to 140% when absorption was
392 measured. The C_p of the CB samples was higher than for the initial sand. Finally,
393 thermal conductivity was slightly lower and this result agrees with the semiempirical
394 relationship developed by Johansen.

395 The second colour process was that described when considering glucose being used
396 as the main black colouring coating substance. The amount of produced coating was
397 quantified as 6% wt. This sample presented higher porosity than the raw silica sand
398 and CB samples. The maximum working temperature for these samples was 441°C.
399 Optical properties increased up to 140% when absorption was measured as in CB
400 sample. The C_p of the glucose sand samples was higher than for the initial sand.
401 Finally, thermal conductivity was slightly lower and this result also agrees with the
402 semiempirical relationship developed by Johansen.

403 In short, both coatings are good candidates in sand particles to be applied in direct
404 particle solar receivers. However, CB coating is more stable, present higher storage
405 capacity (higher C_p), a higher maximum working temperature, and similar optical
406 absorption and physical properties (density and porosity) to the glucose samples.

407 ACKNOWLEDGEMENTS

408 This work has been partially funded by the Spanish government ENE2015-64117-C5-
409 2-R (MINECO/FEDER). The authors would like to thank the Catalan Government for
410 the quality accreditation given to their research group DIOPMA (2017 SGR118). LH
411 and AGF acknowledges the financial support from the Generalitat Valenciana (Project:
412 PROMETEU/2019/079) and from Pla de Promoció de la Investigació a l'UJI (Project:
413 HTF-nano-PCM 16I359). The research was partially supported by EU COST Action
414 CA15119 Nanouptake "Overcoming Barriers to Nanofluids Market Uptake". CB and MJ
415 acknowledges EU COST Action CA15119 for their STMS grants.

416

417

418 REFERENCES

419 [1] C.K. Ho, B.D. Iverson, Review of high-temperature central receiver designs for
420 concentrating solar power, Renewable and Sustainable Energy Reviews 29, 835-846
421 (2014).

422 [2] C.K. Ho, Advances in central receivers for concentrating solar applications, Solar
423 Energy. Article in Press.

424 [3] T. Tan, Y. Chen, Review of study on solid particle solar receivers, Renew. and Sust.
425 Energy Reviews 14, 265-276 (2010).

426 [4] C.K. Ho. A review of high-temperature particle receivers for concentrating solar
427 power. Appl Therm Eng 109, 958–69 (2016).

- 428 [5] Xu C, Wang Z, Li X, Sun F. Energy and exergy analysis of solar power tower plants.
429 Appl Therm Eng 31, 3904–13 (2011).
- 430 [6] Ho CK, et al. Highlights of the high-temperature falling particle receiver project:
431 2012–2016. AIP Conf Proc 1850, 30027 (2017).
- 432 [7] Zhang H, Benoit H, Perez-Lopèz I, Flamant G, Tan T, Baeyens J. High-e \square ciency
433 solar power towers using particle suspensions as heat carrier in the receiver and in the
434 thermal energy storage, Renew Energy 111438–46 (2017).
- 435 [8] Wu W, Trebing D, Amsbeck L, Buck R, P-P. R, Prototype testing of a centrifugal
436 particle receiver for high-temperature concentrating solar applications, J. Energy 137
437 (2015).
- 438 [9] Xiao G, Guo K, Ni M, Luo Z, Cen K. Optical and thermal performance of a high
439 temperature spiral solar particle receiver, Sol. Energy 109, 200-213 (2014).
- 440 [10] Iniesta AC, Diago M, Delclos T, Falcoz Q, Shamim T, Calvet N. Gravity-fed
441 combined solar receiver/storage system using sand particles as heat collector, heat
442 transfer and thermal energy storage media. Energy Procedia 69, 802–11 (2015).
- 443 [11] Martin J, Vitko JJ. ASCUAS: A solar central receiver utilizing a solid thermal
444 carrier. CA (USA): Livermore (1982).
- 445 [12] CK Ho, Highlights of the high-temperature falling particle receiver project: 2012–
446 2016. AIP Conf Proc 1850, 30027 (2017).
- 447 [13] H. Zhang , H. Benoit, I. Perez-Lopez, G. Flamant, T. Tan, J. Baeyens, High-
448 e \square ciency solar power towers using particle suspensions as heat carrier in the receiver
449 and in the thermal energy storage, Renew Energy 111, 438–46 (2017).
- 450 [14] G. Xiao, K. Guo, M. Ni, Z. Luo, K. Cen, Optical and thermal performance of a high
451 temperature spiral solar particle receiver, Sol. Energy, 109:200–13 (2014).
- 452 [15] Siegel NP, Ho CK, Khalsa SS, Kolb GJ, Development and Validation of a
453 Prototype Solid Particle Receiver: On-Sun Testing and Model Validation, ASME J.
454 Solar Energy Engineering 132 (2010).
- 455 [16] Falcone PK, Noring JE, Hruby JM, Assessment of a solid particle receiver for a
456 high temperature solar central receiver system. Livermore, CA: Sandia National
457 Laboratories (SAND85-8208) (1985).
- 458 [17] Ho CK, On-sun testing of an advanced falling particle receiver system. AIP Conf
459 Proc 1734 (2016).
- 460 [18] I. Perez-Lopez, H. Benoit, D. Gauthier, m J.L. Sans, E. Guillot, G. Mazza, G.
461 Flamant, On-sun operation of a 150kW pilot solar receiver using dense particle
462 suspension as heat transfer fluid, Solar Energy 137, 463-476 (2016).
- 463 [19] M. Diago, A. Crespo-Iniesta, A. Soum-Glaude, N. Calvet, Characterization of
464 desert sand to be used as a high-temperature thermal energy storage médium in
465 particle solar receiver technology, Applied Energy 216, 402-413 (2018).
- 466 [20] H. Al-Ansary, A. El-Leathy, S. Jeter, E. Djajadiwinata, S. Alaqel, M. Golob et al.,
467 On-sun experiments on a particle heating receiver with red sand as the working
468 medium, AIP Conference Proceedings 2033 (2018).

- 469 [21] New Mastersizer reduces sample volume for particle size analysis, Metal Powder
470 Report, Volume 70, Issue 1, January– February 2015, Page 47.
- 471 [22] Diffuse Reflectance Accessory Manual. Varian CARY 500 Spectrophotometer.
- 472 [23] G. Ferrer et al., New proposed methodology for specific heat capacity
473 determination of materials for thermal energy storage (TES) by DSC, Journal of Energy
474 Storage 11 (2017) 1-6.
- 475 [24] Smits, K.M., Sakaki, T., Limsuwat, A., Illangasekare, T.H., “Thermal Conductivity
476 of Sands under Varying Moisture and Porosity in Drainage-Wetting Cycles,” Vadose
477 Zone Journal, Volume 9, Number 1, pp. 172-180, (2010).
- 478 [25] Dr. Kamar Shah Ariffin (2004)9 What is Silica? EBS 425- Mineral Perindustrian.
- 479 [26] ASTM International, Standard Tables for Reference Solar Spectral Irradiances:
480 Direct Normal and Hemispherical on 37° Tilted Surface, G173 (2012).
- 481 [27] T. Baumann, S. Zunft. Properties of granular materials as heat transfer and
482 storage medium in CSP application. Sol. En. Mat. and Sol. Cells 143, 38-47 (2015).
- 483 [28] R.H. Perry, D.W. Green, J.O. Maloney. Perry’s chemical engineers’ handbook.
484 McGraw-Hill (seventh edition) (2001).
- 485 [29] H. Kiyohashi, S. Sasaki, H. Masuda. Effective thermal conductivity of silica sand as
486 filling material for crevices around radioactive-waste canisters. High Temperatures- High
487 Pressures 35/36, 179-192 (2004).
- 488 [30] Smits, K.M., Sakaki, T., Limsuwat, A., Illangasekare, T.H., “Thermal Conductivity
489 of Sands under Varying Moisture and Porosity in Drainage-Wetting Cycles,” Vadose
490 Zone Journal, Volume 9, Number 1, pp. 172-180, (2010).
- 491 [31] O. Johansen, Thermal conductivity of soils. Cold regions research and engineering
492 laboratory (1977).

Highlights

- Sand was black coloured through two different methods
- Coloured sands were evaluated as candidates for direct particle solar receivers
- SEM and TGA were used to study coating morphology and its stability with temperature
- The absorption is highly improved for the both black sands compared to the raw sand
- Improvements in C_p and reductions in thermal conductivity were observed

Journal Pre-proof

Declaration of interests

The authors declare that they have no known competing financial interests or personal relationships that could have appeared to influence the work reported in this paper.

The authors declare the following financial interests/personal relationships which may be considered as potential competing interests:

Journal Pre-proof